

Lawrence Berkeley National Laboratory

Recent Work

Title

AN ELECTRON MICROSCOPIC STUDY OF MARGING STEEL

Permalink

<https://escholarship.org/uc/item/8kt5t999>

Author

Cheng, I-Lin.

Publication Date

1967

University of California
Ernest O. Lawrence
Radiation Laboratory

AN ELECTRON MICROSCOPIC STUDY OF MARAGING STEEL

TWO-WEEK LOAN COPY

*This is a Library Circulating Copy
which may be borrowed for two weeks.
For a personal retention copy, call
Tech. Info. Division, Ext. 5545*

Berkeley, California

DISCLAIMER

This document was prepared as an account of work sponsored by the United States Government. While this document is believed to contain correct information, neither the United States Government nor any agency thereof, nor the Regents of the University of California, nor any of their employees, makes any warranty, express or implied, or assumes any legal responsibility for the accuracy, completeness, or usefulness of any information, apparatus, product, or process disclosed, or represents that its use would not infringe privately owned rights. Reference herein to any specific commercial product, process, or service by its trade name, trademark, manufacturer, or otherwise, does not necessarily constitute or imply its endorsement, recommendation, or favoring by the United States Government or any agency thereof, or the Regents of the University of California. The views and opinions of authors expressed herein do not necessarily state or reflect those of the United States Government or any agency thereof or the Regents of the University of California.

Research and Development

UCRL-17334

UNIVERSITY OF CALIFORNIA
Lawrence Radiation Laboratory
Berkeley, California

AEC Contract W-7405-eng-48

AN ELECTRON MICROSCOPIC STUDY OF MARAGING STEEL

I-Lin Cheng
(M. S. Thesis)

January 1967

AN ELECTRON MICROSCOPIC STUDY OF MARAGING STEEL

I-Lin Cheng

Inorganic Materials Research Division, Lawrence Radiation Laboratory,
and Department of Mineral Technology, College of Engineering,
University of California, Berkeley, California

March 1967

ABSTRACT

A careful examination of one system of maraging steels based on Ni-Co-Ti-Fe has been done primarily using electron microscopy, in an attempt to delineate the hardening mechanism in terms of the substructural changes.

The results indicated that precipitation hardening is the main strengthening mechanism. Upon plastic deformation, the specimens exhibited a brittle failure under typical maraging treatments which gave microstructures having grain and/or martensite sub-boundary precipitation. Identification of precipitates by electron diffraction and electron beam microprobe indicated that they were a (Ni-Ti) intermetallic compound, probably, Ni_3Ti . The orientation relationship of them with the matrix is $(001)_\eta // (110)_\alpha$, $[2\bar{1}\bar{1}0]_\eta // [1\bar{1}1]_\alpha$.

An analysis is made using both the Orowan and Ansell models to account for the initial yield stress of this alloy. It is concluded that the Ansell model is the controlling one.

I. INTRODUCTION

Because of their superior high strength,¹ ductility,¹ high temperature creep resistance² and low temperature properties,³ maraging steels have become one of the most promising materials for structural purposes.

The high nickel, low carbon, alloy steel, when annealed and quenched, can produce a relatively soft ($R_c 25$) and ductile B.C.C. martensite. Upon reheating or aging, intermetallic compounds, instead of carbides, precipitate out from the supersaturated solution. It was precipitation which was thought to be responsible for the major hardening mechanism.^{4,5} Recently, Mihalisin⁶ utilized neutron diffraction analysis and found, besides precipitation hardening, that ordering might also play a role in strengthening.

Here a simpler system of maraging steel of Fe-Ni-Co-Ti was studied in order to delineate the hardening mechanism more clearly. The changes in microstructures with mechanical properties were related. The orientation relationship between the matrix and precipitates was determined using selected area electron diffraction of the thin foils. Identification of the precipitates was done by using an electron microprobe analyzer and x-ray microanalyzer on overaged samples.

II. EXPERIMENTAL

The material used for this study was supplied by International Nickel Company as a hot rolled bar. The chemical composition is given in Table I.

The bar was hot rolled with intermediate annealing down to 25 mils. Further reduction to produce foils suitable for electron microscopy work was done by cold rolling to 10 mils. thickness.

TABLE I
Chemical Analysis

Composition, wt. %						
Ni	Co	Al	Ti	C	Fe	
20.3	23.6	0.068	0.17	0.055	Balance	

A. M_s Determination

The measurement of transformation temperature during heating and cooling was done by using a differential thermal method. As shown in Fig. 1, two specimens, one the steel sample and the other a nickel sample, which acted as a dummy because it possessed no transformations in the temperature range investigated, were spark welded to two separate chromel-alumel thermocouples. Two temperature recorders were used, one for the temperature and one for the differential temperature. The transformation temperatures were observed whenever there was a peak in the differential temperature curves.

B. Heat Treatment

The samples were vacuum sealed in quartz tubes and solution treated at 2100°F for 4 hours. Four different cooling rates were used, namely, furnace, water, air and liquid nitrogen. The aging treatments were performed on all of the four cooling rate specimens, using 700F and 900F as aging temperatures, since this is the temperature range which was thought of interest.

C. Mechanical Tests

Rockwell hardness was measured for each as-quenched and aged sample.

Tensile tests were carried out on an Instron machine with a cross head speed of 0.05 cm/min.

D. X-Ray

Using a XRD-3 diffractometer with vanadium filtered chromium radiation, the volume percentage of austenite was determined by direct comparison of the integrated intensity of an austenite line with that of a martensite line.

E. Microprobe

Electron microprobe analysis was made by using an MAC Model 400 Electron Microprobe Analyzer on an overaged specimen and Siemens x-ray XMA microanalyser in conjunction with electron microscopy using carbon extraction replicas.

F. Microscopy

Specimens prepared for optical microscopy were mechanically polished with emery papers and etched in ferric chloric acid. Extraction replicas were prepared by depositing carbon on etched specimens (etchant 15 ml HCl, 10 ml acetic acid, 10 ml HNO₃, and a few drops of glycerine) and removing the carbon film by subsequent etching. Thin foils for electron microscope were prepared by chemical and electro-polishing. 10 mil specimens were chemically thinned in a H₂O₂-H₃PO₄ bath to about 3 mils. Electro-polishing was performed utilizing the "window" method in an electrolyte of 90% glacial acetic acid and 10% perchloric acid with an applied voltage of about 20 V DC. All the replicas and thin foils were observed in a Siemens Elmiskop IA microscope with an operating condition of 40 KV for x-ray microanalysis and 100 KV for replicas and thin foils.

Dark field techniques were performed to study and reveal the precipitates.

Preliminary identification was performed by inserting the objective aperture on the precipitate diffraction spots. However, for the best resolution, gun tilting is necessary to avoid spherical aberration.

III. RESULTS AND DISCUSSION

A. Transformation Temperature

The range of ferrite austenite transformation temperature α - γ , or As-Af, as determined by the differential thermal method, was found to be 1400°F-1620°F, and the martensite transformation temperature 690°F-540°F. The latter was obtained by furnace cooling samples with a cooling rate of about 4.8°C/min. Since it has been found that cooling rates had no significant effect on the M_S temperature for the Fe-Ni alloys,⁷ it is concluded that M_S temperatures do not differ appreciably from one another by the four kinds of cooling studied. The martensite transformation temperature was higher than that observed from the iron-nickel binary alloy transformation diagram. This is expected because of the high cobalt and low carbon content of this alloy and the fact that cobalt tends to raise the M_S temperature whereas carbon lowers the M_S temperature.

B. As Quenched State

All the samples from different cooling rates showed mainly a BCC structure after quenching, as revealed by both optical and electron micrographs in Fig. 4. No acicular feature characteristic of martensite was observed in the optical micrograph, but blocky, irregular ferrite grains which is usually referred to as "massive martensite".⁸ In the thin foil electron micrographs, laths of martensite grains were observed which contain a high dislocation density in a form of tangles or irregular structure, which

presumably arise as a result of the shear transformation ($\gamma\text{-}\alpha$) of the material. No internal twinning was observed. This is consistent with the fact that M_s temperature of this alloy is high and the readily visible dislocation substructures within martensite grains.¹⁰ Some of the martensite laths were twin related as can be detected from the select area diffraction pattern from two adjacent grains.

In the electron micrographs, the martensite "laths" appear to be parallel with slight misorientation. Bundles of these laths are thought to produce the blocky structure as seen in the optical micrograph.

There were no substantial differences in the quenched structure among these four treatments, except the liquid nitrogen cooling specimen showed narrower martensite laths which might be responsible for the higher hardness and yield stress observed after this treatment (Fig. 2 and Table II). The strength of the as-quenched martensite is due, principally, to the solid solution hardening combined with the work hardening contributions from transformation substructure. The high ductility of martensite produced is presumably due to the low carbon content (which reduces the brittleness of this phase just as it does in plain carbon steels), the absence of any precipitates,* and the high dislocation density.

The orientation relationship between martensite and austenite could not be obtained because of the relatively small amount of austenite remaining after quenching, as revealed by x-ray diffraction analysis.

Finally, the "burst" formation of martensite needles could be revealed from the differential temperature curves in the transformation temperature determination which showed serrated peaks as the M_s temperature was reached.

*No precipitation was detected in as-quenched martensitic structures, even after many attempts to detect them using dark field techniques.

C. Aged State

1. Mechanical Properties

The changes of properties resulting from different aging conditions were measured at room temperature and the results are shown in Table II and Figs. 2 and 3. It is seen from Fig. 2 that the hardness increases very rapidly and the form of hardness -time curves follows those of precipitation hardening alloys, i.e., maximum hardness occurs at longer times as the aging temperature is lowered (700F vs 900F). The yield and ultimate tensile strength increases, but there is a loss in ductility, as shown in Fig. 3. Also, the suggested typical maraging treatment,¹ 900F + 3 hours aging was not suitable for this alloy. All the specimens in the 900F aging treatment appeared to fail in a brittle manner with an intergranular fracture²⁴ before yielding. This phenomenon will be discussed in association with the microstructural changes. Higher work hardening rates were also observed from the stress-strain curves (Fig. 3) as the aging progresses.

2. Identification of Precipitates

Qualitative chemical analysis by x-ray microanalysis and electron beam probe showed that the precipitate is composed to nickel and titanium. As shown in Fig. 5, the extracted precipitates show an Ni peak mounted on a Ti grid and a Ti peak as mounted on an Ni grid, when examined on the electron microscope using x-ray microanalysis.* Also, in Fig. 6, it is seen that, in the overaged conditions, the precipitates grow into the size which is detectable in the optical microscope and the electron beam probe using $TiK\alpha$ showed some agglomerates of Ti. In this case,

*The XMA has been calibrated before analyzing the precipitates. See Appendix II.

because of the thickness of precipitates and penetration of the electron beam, the Ni content of the precipitate was difficult to determine because Ni together with Fe + Co is the abundant element in the matrix.

Fig. 7a shows an electron micrograph of the carbon extraction replica from a sample overaged at 600°C for 19 1/2 hrs., which showed a Rockwell hardness of only Rc₂₄. Compared with the thin foil micrograph in Fig. 7b, the larger plates are probably the precipitates along former martensite boundaries, the rest being distributed uniformly throughout the matrix. During overaging, some austenite reformed. The little dots on the replica micrograph are presumed to be due to this phase. This deduction has been confirmed by examinations of other replicas²⁴ which were free of precipitates, but which also showed the same "dot" structure, and by austenite rings that were identified on a diffraction pattern.

Fig. 7c is the selected area diffraction pattern from Fig. 7a. The "d" spacings from the selected area diffraction pattern of the thin foil (not shown here), and the relative intensities of the reflections, are shown in Table III. Comparing these data with x-ray powder data for Ni₃Ti yields a reasonable match. The precipitates are thus tentatively identified within the limits of electron diffraction as Ni₃Ti hexagonal phase with a DO₂₄ structure.

In some cases, rectangular particles were extracted²⁴ and these particles were tentatively identified as TiC or TiN by means of their selected area diffraction pattern. The crystal structures of TiC and TiN are identical and they have similar lattice parameters, so, as Reisdorf has suggested,¹² Ti (C,N) is used to indicate this compound.

3. Observations of the Maraging Structure

Observations of the maraged structure were done exclusively by electron microscopy, since no evidence of precipitation and only dark etching along the grain boundaries were observed in the optical microscope.

700F Aging

During the early stage of aging, e.g., 15 minutes, no precipitation could be detected in the photomicrograph. However, in the diffraction pattern, faint streaks through the matrix diffraction spots were observed, which may indicate plate-like or disc-shaped "precipitates" with the streaking direction perpendicular to the plane of the "clusters". This is quite reasonable, since it is often possible to detect the evidence of solute atom clustering or G.P. zones in the diffraction patterns before a precipitate can be easily seen in the microstructure. Also, because of the difference in atomic size of the matrix and precipitate, an elastic distortion of the matrix would also produce diffraction effects. This gives rise to some streaking of the lattice points in a direction parallel to the distortion, except for the central spot.¹³ No strain contrast of matrix could be revealed on the photograph, probably because the strain contrast is too small to be resolved and of complexities due to incoherent scattering from the high dislocation density. After the 3 hours aging treatment, small particles could be detected in the bright field image, but they were rather obscure because of the high dislocation density. However, in the dark field image produced by gun tilting, the presence of precipitates is quite obvious as Fig. 8 shows. The precipitates have an average diameter of about 180-200Å. The precipitates are uniformly distributed throughout the matrix which suggests that they may have formed

on the dense dislocation structure produced during the martensitic transformation. Precipitation on dislocations is generally favored because some of the strains resulting from the differences in lattice parameter of the precipitates and matrix can be relaxed. In addition, the precipitate atoms diffuse more rapidly along the dislocations as a result of "pipe diffusion" and this accelerates aging. The precipitates begin to grow, having definite orientations and having a tendency to segregate on the martensite sub-boundaries in an aging time of 12 hours (as compared to 3 hours previously). This can be seen in Fig. 9, especially in dark field photomicrography. The precipitates become larger at longer aging times. Because martensite boundaries and grain boundaries provide better sites for the precipitation, boundary precipitation occurs and boundary particles grow much larger than those in the matrix (Fig. 10c).

900F Aging

Aging for 1 hour at this temperature caused extensive grain boundary precipitation along former martensite boundaries, as in Fig. 10. This kind of precipitation should have a significant affect on the toughness of this alloy and will be discussed later. Aging for 3 hours, which is the suggested typical treatment, produced both the matrix and boundary precipitation, although the boundary precipitates grow faster than those in the matrix. Dark field photomicrographs, as shown in Fig. 11, usually indicate the size and direction of the matrix precipitates, while the boundary precipitates are usually in different orientations. Rather strong precipitate diffraction spots produced in the diffraction pattern are thought to be responsible for the dark precipitate contrast in the

bright field micrograph. Twelve hours aging at this temperature caused some formation of subgrains due to recovery and recrystallization besides growth of precipitates (Fig. 12).

4. Morphology of Precipitates and their Orientation Relationship with the Matrix.

Because of streaking in the diffraction pattern, it is seen that the shape of the precipitate is either disc-like or plate-like (due to relaxation of Laue diffraction condition in one dimension). This is confirmed in the micrograph shown in Fig. 11, where the projections of the precipitates on (110) plane show rectangular shapes. Analysis of the diffraction patterns showed that the precipitates lie on {110} planes of the matrix. As indicated by Pitter and Ansell,¹⁴ the Ni_3Ti is a hexagonal phase and has an orientation relationship with the matrix such that $(0001)_\eta // (110)_\alpha$ and $[2\bar{1}10]_\eta // [1\bar{1}1]_\alpha$. The relationship is confirmed in this investigation, and an example is shown in Fig. 13.

5. Reversion of Austenite

The amount of austenite was determined by using the formula:¹⁵

$$\text{volume \% austenite} = \frac{100}{1 + (1.7) \left(\frac{I_\alpha}{I_\gamma} \right)}$$

where I_α = integrated intensity of (200-002) martensite x-ray line.

I_γ = integrated intensity of (200) austenite line.

The value of "1.7" was calculated in the appendix.

The results are given in Table IV. It is seen that upon aging the amount of austenite gradually increases. This phenomenon is thought to be due to the reversion of the metastable BCC phase to the equilibrium austenite and ferrite phases because of the rise in M_s temperature resulting from depletion of Ni from the matrix as a result of precipitation.

Overaging by aging at 1100°F for 19.5 hours caused softening of this alloy (Rc 25). This phenomenon is related with the amount of austenite present which is rather high (39.4%). Examination of thin foils of the overaged specimen revealed dots or small lumps of particles which were determined to be austenite by electron diffraction analysis. Hence, it was concluded that overaging occurred primarily because of austenite reversion (with a concurrent slight growth of precipitates).

There appears to be a critical amount of austenite at which the softening occurs. In the usual maraging treatment, although the amount of austenite increases, its softening effect is overshadowed by the precipitation hardening effect.

6. Structural Changes and Mechanical Properties

The high ductility observed in the as-quenched state is thought to be related to the low carbon content (which eliminates the brittleness characteristic which exists in plain carbon steels), and the high dislocation density introduced during transformation. Combining with its softness, the martensitic product may exhibit good machinability and formability prior to any aging treatment.

In these experiments, it was found that the ductility decreased with aging time and/or temperature. Careful examination of the substructures showed that there was a strong tendency for grain boundary segregation of precipitates to occur and this was associated with a marked decrease in the ductility, (e.g. 700F/12 hrs aged specimen) as in Fig. 9. Also, some of the specimens broke in the grips which indicated a noticeable notch sensitivity. This brittleness feature has been indicated by Floreen and Speich¹⁷ as due to grain boundary embrittlement in the absence of Mo.

They showed by carbon replica fractographs of the surfaces of fractured Charpy bars that the molybdenum-containing alloy showed a dimpled-type fracture surface characteristic of ductile fracture, whereas the brittle titanium containing alloy showed a flat fracture surface typical of a brittle intergranular fracture. This is consistent with experiments now in progress.²⁴ Preferential precipitation along the boundaries, i.e., both grain boundaries and sub-boundaries, makes the boundaries stronger. Thus, the dislocations cannot easily cross the boundaries to continue the deformation and have a tendency to pile up against the boundaries until the internal stresses set up are large enough to break or shear the precipitates on the boundaries. This phenomenon is clearly shown in Figs. 16, 15 and 16 where the bending and/or shearing of particles can be seen. It is also interesting to note that the precipitates in the matrix are relatively undeformed and the shearing directions of the boundary precipitates are $\langle 111 \rangle$, i.e., the slip direction in BCC metals.

In addition, the presence of Ti(C,N) particles, as extracted on replicas in this research,²⁴ may also be a factor causing low notch toughness of this alloy.¹⁸

The increasing work hardening rate occurring during the aging treatment is thought to be due to the resistance to dislocation motion by precipitates or by multiplication of dislocations as a result of dislocation precipitate interactions.

D. Strength of Maraging Steels

There are three factors which are thought to control the hardening mechanism. Namely, dispersion hardening, ordering, and martensitic grain size. Another factor is the carbon content, which in the present alloy

is rather small so that its contribution to hardening may be neglected as compared to the other parameters.

1. Dispersion of Precipitates

Several theories have been proposed to account for the yield stress of precipitation hardenable alloys.¹⁹ Orowan suggested that the plastic strain results from the expansion of dislocation loops surrounding particles which intersect the glide plane. Ansell and Lenel²⁰ suggested that detectable plastic flow would occur only when the particles are being sheared or broken by the passing dislocations. Dislocations pile up against second-phase particles and the particles rupture whenever the accumulated stress is large enough. These two theories will be tested separately as follows:

a. Orowan type:

The modified Orowan relationship is that the initial shear yield stress should be given by:

$$\tau = \tau_s + \frac{Gb}{4\pi} \phi \ln \left\{ \frac{d-2r}{2b} \right\} \frac{1}{(d-2r)/2} \quad (1)$$

where

G = shear modulus of the matrix = 7300 Kg/mm².

τ_s = initial yield stress of the matrix, take the value of as-quenched state, = 53,500 psi.

b = Burgers vector = 2.49Å

r = mean particle radius = 90 ~ 120Å

d = mean planar interparticle spacing = 400 - 500Å

$\phi = 1/2(1 + 1/1-\nu)$. ν = Poisson's ratio = 0.3. $\phi = 1.215$

The above values are based on the aging condition of 700F/3 hrs, where the yield stress and precipitates were detectable. Using

the above values, we obtain $\tau = 140,000$ psi.

b. Ansel-Lenel type:

The final form of Ansell and Lenel's model is that the yield stress of a dispersion hardened material should be:¹⁹

$$\tau = \tau_s + \frac{G'}{4c} \frac{f^{1/3}}{(0.82 - f^{1/3})} \quad (1)$$

where

τ_s : yield stress of the matrix, take $\tau_s = 53,500$ as previously.

G' : shear modulus of the Ti-Ni phase,²³ 8.9×10^6 psi.

C : a constant approximately equal to 30.

f : volume fraction of particles approximately equal to 5.2% (for spherical particles $\frac{r}{R} = \frac{f^{1/3}}{0.82}$ where r is radius of particles and $2R$ mean separation between particles).

Hence, we obtain an initial yield stress of 110,000 psi.

Comparing the results from these two models with the experimental determination value, which showed a tensile yield stress of 192,000/2 psi,* or shear yield of 96,000 psi, it is suggested that the Ansell's model may be the plausible one. In addition, the observation of particle shearing after further aging (Fig. 15) may confirm Ansell's model.

2. Ordering

Although the precipitated phase Ni_3Ti (Do_3 or Do_{24}) is ordered, the matrix also has a tendency to be ordered.²¹ In view of the composition of this alloy, Fe-Ni and Co may combine to form an ordered phase. Mihalish,⁶ using neutron diffraction, did observe ordering of this type of alloy in

*By assuming that the tensile yield stress is about twice the shear stress.

which the ordered phase had a composition near Fe_2CoNi . In the present work, an attempt was made to find the existence of superdislocation which would indicate order,²² but there seemed no such evidence. Hence, the effect due to ordering may be small.

3. Martensitic Grain Size

It was observed in this alloy that in liquid nitrogen cooling state, the hardness and yield strength are higher than the other quenching medium. This was explained as due to the finer martensitic grain size as observed in the electron microscope, although no such tendency observed by optical microscope.

Finally, it should be noted that the strength in the as-quenched state is controlled partly by the high dislocation density existing. During the subsequent aging, the dislocations annealed out gradually due to recovery, as was observed in the electron microscope, (Fig. 17) and thus the contribution from the dislocation density decreased as the precipitation hardening mechanism became more effective.

IV. CONCLUSIONS

1. The structures are relatively insensitive to cooling rates, a b.c.c. massive martensite was produced in each case, i.e., the cooling rate does not effect the M_s transformation temperature appreciably in this alloy.
2. The martensite platelets produced by quenching are relatively soft and contain a high dislocation density. Low carbon content and high dislocation density may be responsible for their ductility. The low work hardening rate in this state may account for the fact that the

dislocation density already is so high that the martensite is in a work hardened state.

3. The precipitates were identified as Ni_3Ti , which is a hexagonal phase. The precipitates are formed as thin plates and are oriented with the martensite matrix such that $(0001)_\eta // (110)_\alpha$ and $[2\bar{1}\bar{1}0]_\eta // [\bar{1}\bar{1}1]_\alpha$.

4. Grain boundary precipitation causes brittleness of this alloy. The fractured surface showed an intergranular fracture. The existence of $\text{Ti}(\text{C,N})$ particles may be an additional factor in embrittling.

5. Grain boundary precipitates break or shear as the stress from the surrounding dislocation groups becomes large enough. Precipitates are sheared in the $\langle 111 \rangle$ slip directions of the matrix.

6. The strength of maraging steels is due primarily to dispersion hardening. The Ansell model of yielding is probably the operating mechanism.

7. Softening occurs when the amount of austenite reversed exceeds a certain critical value, under which the age-hardening effect overrides. Overaging is thus due to reversion of austenite with little appreciable growth of precipitates.

8. Upon aging, the dislocation density decreases as a result of recovery.

9. Although high strength can be obtained in this alloy, it is not very promising because of its low ductility. Hence, the prevention of boundary precipitation, e.g., the beneficial addition of Mo, may improve the properties greatly.

which the ordered phase had a composition near Fe_2CoNi . In the present work, an attempt was made to find the existence of superdislocation which would indicate order,²² but there seemed no such evidence. Hence, the effect due to ordering may be small.

3. Martensitic Grain Size

It was observed in this alloy that in liquid nitrogen cooling state, the hardness and yield strength are higher than the other quenching medium. This was explained as due to the finer martensitic grain size as observed in the electron microscope, although no such tendency observed by optical microscope.

Finally, it should be noted that the strength in the as-quenched state is controlled partly by the high dislocation density existing. During the subsequent aging, the dislocations annealed out gradually due to recovery, as was observed in the electron microscope, (Fig. 17) and thus the contribution from the dislocation density decreased as the precipitation hardening mechanism became more effective.

IV. CONCLUSIONS

1. The structures are relatively insensitive to cooling rates, a b.c.c. massive martensite was produced in each case, i.e., the cooling rate does not effect the M_s transformation temperature appreciably in this alloy.
2. The martensite platelets produced by quenching are relatively soft and contain a high dislocation density. Low carbon content and high dislocation density may be responsible for their ductility. The low work hardening rate in this state may account for the fact that the

dislocation density already is so high that the martensite is in a work hardened state.

3. The precipitates were identified as Ni_3Ti , which is a hexagonal phase. The precipitates are formed as thin plates and are oriented with the martensite matrix such that $(0001)_\eta // (110)_\alpha$ and $[2\bar{1}\bar{1}0]_\eta // [\bar{1}\bar{1}]_\alpha$.

4. Grain boundary precipitation causes brittleness of this alloy. The fractured surface showed an intergranular fracture. The existence of $\text{Ti}(\text{C,N})$ particles may be an additional factor in embrittling.

5. Grain boundary precipitates break or shear as the stress from the surrounding dislocation groups becomes large enough. Precipitates are sheared in the $\langle 111 \rangle$ slip directions of the matrix.

6. The strength of maraging steels is due primarily to dispersion hardening. The Ansell model of yielding is probably the operating mechanism.

7. Softening occurs when the amount of austenite reversed exceeds a certain critical value, under which the age-hardening effect overrides. Overaging is thus due to reversion of austenite with little appreciable growth of precipitates.

8. Upon aging, the dislocation density decreases as a result of recovery.

9. Although high strength can be obtained in this alloy, it is not very promising because of its low ductility. Hence, the prevention of boundary precipitation, e.g., the beneficial addition of Mo, may improve the properties greatly.

10. It is suggested that ausforming prior to transformation to martensite of maraging steels may accelerate the aging response by introducing more dislocations, and increase the strength by having more uniformly distributed precipitates upon subsequent aging.

APPENDIX I

Calculations of volume % austenite with negligible amounts of third phase, the volume percent of austenite is determined by:

$$\%Y = \frac{100}{1 + \left(\frac{R_Y}{R_\alpha}\right) \left(\frac{I_\alpha}{I_Y}\right)}$$

$$\frac{R_Y}{R_\alpha} = \frac{V_\alpha^2 F_Y^2 P_Y [(1 + \cos^2 2\theta) / (\sin^2 \theta \cos \theta)]_Y [\exp(-2m)]_Y}{V_Y \delta F_\alpha^2 P_\alpha [(1 + \cos^2 2\theta) / (\sin^2 \theta \cos \theta)]_\alpha [\exp(-2m)]_\alpha}$$

where F is the absolute value of the structure factor, P is the multiplicity factor, V is the volume of unit cell, exp(-2m) is the temperature factor and $\frac{1 + \cos^2 2\theta}{\sin^2 \theta \cos \theta}$ = Lorentz polarization factor.

Factor	Martensite (200-002)	Austenite (200)
2θ	106.2	79.4
θ	53.1	39.7
$\frac{1 + \cos^2 2\theta}{(\sin^2 \theta \cos \theta)}$	2.815	3.293
sinθ/λ	0.35	0.279
F ²	4(14.62) ²	16(16.50) ²
P	4+2	6
exp(-2m)	0.91	0.94
V ²	(2.866) ⁴ (2.873) ²	(3.557) ⁶

The ratio $\frac{R_Y}{R_\alpha}$ is thus calculated from the above values: $\frac{R_Y}{R_\alpha} = 1.7$

APPENDIX II

CALIBRATION DATA FOR THE XMA⁺

(the emission lines of the metals listed below ere excited with the continuous x-radiation of a Pt target and were monochromatized with a Li-F crystal)

x-ray unit voltage- current KV-MA	"Z"	Element	Peak Position		Resolution(%)**	Peak Width 1/2 Max. Intern (Kev)
			Theoretical	Experimental*		
40-5***	22	Ti	4.51	4.42	20.3	0.90
35-1	26	Fe	6.40	6.41	17.2	1.10
30-1	27	Co	6.93	6.96	16.4	1.14
35-1	28	Ni	7.48	7.56	15.3	1.16
26-1	28	Ni(no mono chromator	7.48	7.44	17.5	1.30
50.5****	40	Zr	15.77	15.90	11.1	1.76

* To obtain the energy from a peak position on the PHA, the scale is so clibrated that you read the volts on the discriminator (0-100 volts) and multiply by 0.2.

** Defined as $\frac{(\Delta V) \text{ at } 1/2 I_{\max}}{V \text{ at } I_{\max}} \times 100$

*** It takes a lot of intensity to get a detectable amount of Ti K_a x-rays through the Mylar window of the flow counter, so I have my doubts about Aluminum.

**** The opposite problem: insufficient quantum yield to activate the flow counter.

+ By E. A. Sturken

ACKNOWLEDGEMENTS

The author is deeply grateful to Professor Gareth Thomas for his encouragement, guidance and support during this research. Special thanks are due to Professor E. R. Parker for reviewing this thesis. I wish also to thank P. Mangonon, E. Sturken and G. Georgakopoulos for some helpful suggestions during this experiment.

This work was done under the auspices of the United States Atomic Energy Commission through the Inorganic Materials Research Division of the Lawrence Radiation Laboratory.

TABLE II

Tensile Properties*

Treatment (2100F/4h Annealing)	Yield (0.2%) Ksi	Ultimate Ksi	Elongation %
LN As Quenched	107	132	6.1
LN 700F/1/4h	150	175	5.0
LN 700F/1h	166	185	2.7
LN 700F/3h	192	192	2.0
LN 700F/12h ⁺			
WC As Quenched	98	112.2	7.2
WC 700F/1/4h	147	164.5	4.8
WC 700F/1h	162	177.5	3.6
WC 700F/3h	168	186	2.2
WC 700F/12h ⁺			
FC As Quenched	96	114	6.5
FC 700F/1/4h	120	137.5	5.2
FC 700F/1h	145	151	4.1
FC 700F/3h	153	160	2.9
FC 700F/12h ⁺			
AC As Quenched	97.5	120	6.2
AC 700F/1/4h	131	140	4.9
AC 700/1h	147	156	3.9
AC 700F/3h	155	163	2.7
AC 700F/12h ⁺			

*All the 900F aging specimens broke before yielding.

+Broken before yielding.

TABLE III

Interplanar Spacings of the Precipitates
(2100/4h Annealing, LN cooling, 600°C/19 1/2h aged)

Thin Film		Replica (Ring Patterns)	Austenite [§]	Martensite	Ni Ti() [†]		
d(Å)	I/I ₀ *	d(Å)	d(Å)	d(Å)	d(Å)	I/I ₀	(hk)
2.21	M	2.21			2.21	20	200
2.14	M	-----			2.13	50	201
2.075	S	-----	2.08	2.027	2.07	50	004
1.943	VS	1.95			1.95	100	202
1.83	M	-----		1.83			
-----		-----			1.72	20	203
-----		-----			1.54	10	122
-----		-----		1.43	1.51	20	204
1.35	M	-----	1.37		1.330	20	205
1.26	S	1.273			1.276	50	220
1.16	M	1.16		1.17	1.173	20	206
1.09	M		1.09		1.095	10	401
-----		-----			1.087	50	224
1.06	M	1.06			1.068	50	402
-----		-----			1.046	20	207
1.032	W	-----			1.038	20	008
-----		-----		1.013	1.027	20	403
0.973	W	-----			0.974	10	404
0.94	W	0.94			0.940	10	226,412
-----		-----		0.906	0.920	10	405
0.85	W	0.85	0.85		0.831	10	421
-----		-----			0.819	20	422
-----		-----			0.800	10	423
0.775	W	-----			0.779	10	505,414

*VS(very strong), S(Strong), M(Medium, W(Weak)

†ASTM x-ray powder data file.

§By x-ray diffraction

TABLE IV

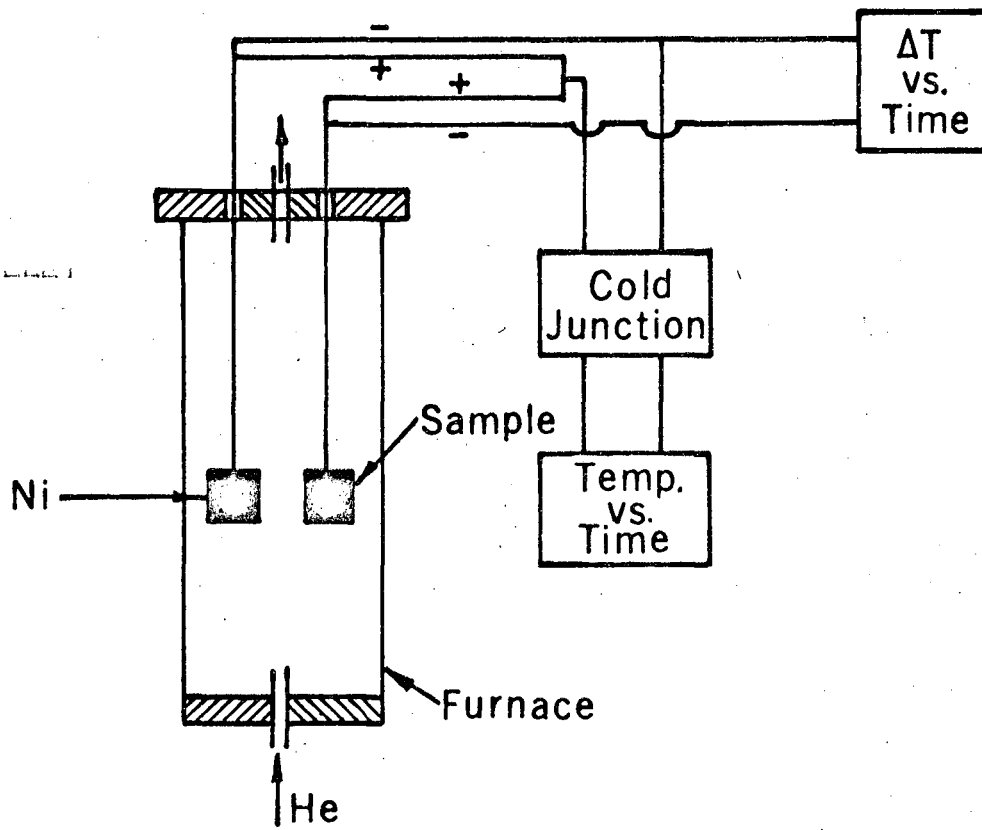
Amount of Retained Austenite

Treatment	% Austenite
As Quenched (LN)	1.5
700F/ 1/4 hr	3.57
700F/ 1 hr	8.34
700F/ 3 hrs	8.93
700F/ 12 hrs	14.15
900F/ 1/4 hr	4.50
900F/ 1 hr	9.05
900F/ 1 hr	9.05
900F/ 3 hrs	13.30
900F/ 12 hrs	27.00
1100F/ 19.5 hrs	39.40

REFERENCES

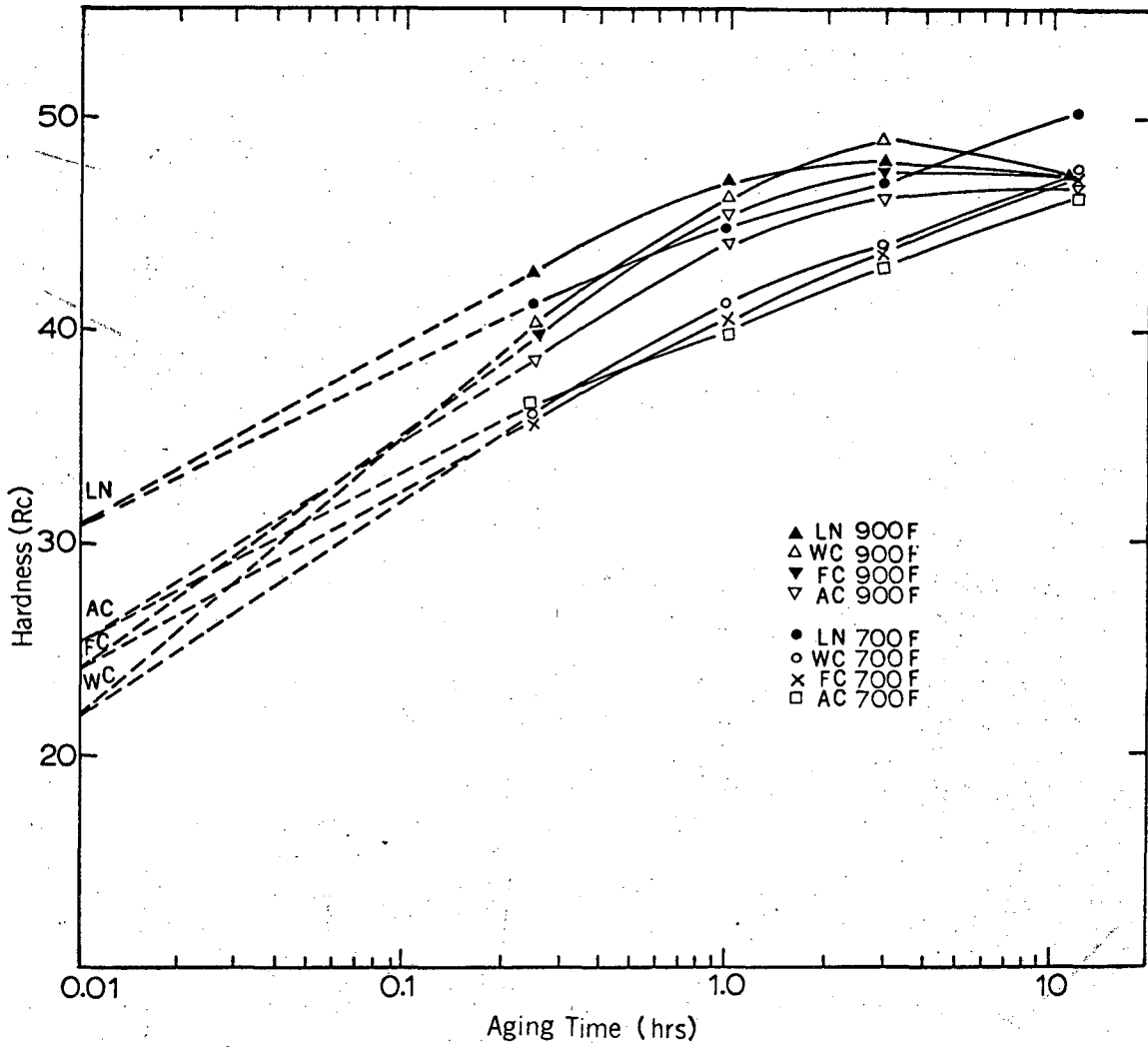
1. R. F. Decker, J. T. Eash, and A. J. Goldman, "18% Nickel Maraging Steel", ASM trans Quart, 55 58 (1962).
2. S. Floreen and R. F. Decker, "Maraging Steel for 100F Service", ASM Trans Quart, 56 403 (1963).
3. R. H. Bush, "Mechanical Properties of an Ausformed Maraging Steel", ASM Trans Quart, 56, 885 (1963).
4. A. J. Baker and P. R. Swann, "The Hardening Mechanism in Maraging Steels", ASM Trans Quart, 57, 1009 (1964).
5. G. P. Miller and W. I. Mitchell, "Structure and Hardening Mechanisms of 18% Ni-Co-Mo Maraging Steels", J. Iron Steel Inst., 203, 899 (1965).
6. J. R. Mihalisin, "Age Hardening and Structure of Iron-Nickel-Cobalt Alloys", ASM Trans Quart, 59, 60 (1966).
7. A. Gilbert and W. S. Owen, "Diffusionless Transformation in Iron-Nickel, Iron-Chromium and Iron Silicon Alloys", Acta Met., 10, 45 (1962).
8. G. P. Miller and W. I. Mitchell, "Structure of Nickel-Cobalt-Molybdenum Maraging Steel in the Air-Cooled Condition", J. Iron Steel Inst., 203, 895 (1965).
9. O. Johari and G. Thomas, "Factors Determining Twinning in Martensite", Acta Met., 13, 1211 (1965).
10. P. M. Kelly and J. Nutting, "The Morphology of Martensite", J. Iron Steel Inst., 199 (1961).
- 11a. G. R. Speich and P. R. Swann, "Yield Strength and Transformation Substructure of Quenched Iron-Nickel Alloys", J. Iron Steel Inst. 203, 480 (1965).
- 11b. O. Johari and G. Thomas, "Structure and Strength of Ausformed Steel". Trans ASM 58, 563 (1965).

12. B. G. Reisdorf, "Identification of Precipitates in 18, 20 and 25% Nickel Maraging Steels", ASM Trans Quart, 56 783 (1963).
13. Hirsch, Howie, et. al., "Electron Microscopy of Thin Crystals", Butterworths, 1965, p. 320.
14. R. K. Pitler and G. S. Ansell, "Precipitation in High Nickel Maraging Steel", ASM Trans Quart., 57, 220 (1964).
15. H. R. Erard, "Advances in X-Ray Analysis", ed. by W. M. Mueller et. al., Plenum Press, N.Y. pp. 256.
16. B. D. Cullity, "Elements of X-Ray Diffraction", Addison-Wesley Publishing Company, Inc. pp. 391.
17. S. Floreen and G. R. Speich, "Some Observations of the Strength and Toughness of Maraging Steel", ASM Trans Quart., 57, 714 (1964).
18. A. J. Birkle et. al., "A Metallographic Investigation of the Factors Affecting the Notch Toughness of Maraging Steels", ASM Trans Quart 58, 285 (1965).
19. A. Kelly and R. B. Nicholson, Prog. Mater. Sci., 10 336 (1963).
20. G. S. Ansell, "Fine Particle Effect in Dispersion-Strengthening", Acta Met., 9 518 (1961).
21. C. G. Shull and S. Siegel, "Neutron Diffraction Studies of Order-Disorder in Alloys", Phys. Rev. 75.
22. W. Bell, W. R. Roser and G. Thomas, "Diffraction Analysis of Dislocation Pairs for Detecting Order in Solid Solutions", Acta Met., 12 1247 (1964).
23. W. J. Buehler and R. C. Wiley, "Ti-Ni Ductile Intermetallic Compound", ASM Trans Quart, 55 269 (1962).
24. I-Lin Cheng and G. Thomas, unpublished work.



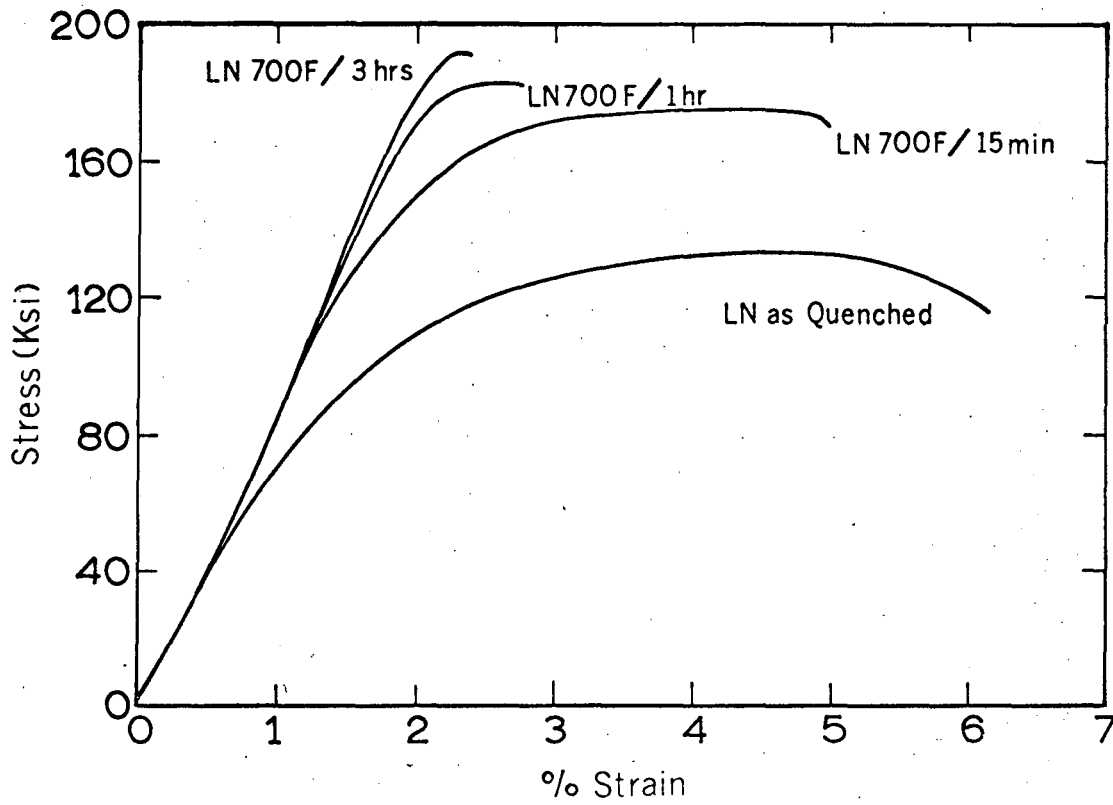
MUB-13759

Fig. 1 Thermal differential apparatus for measuring transformation temperatures.



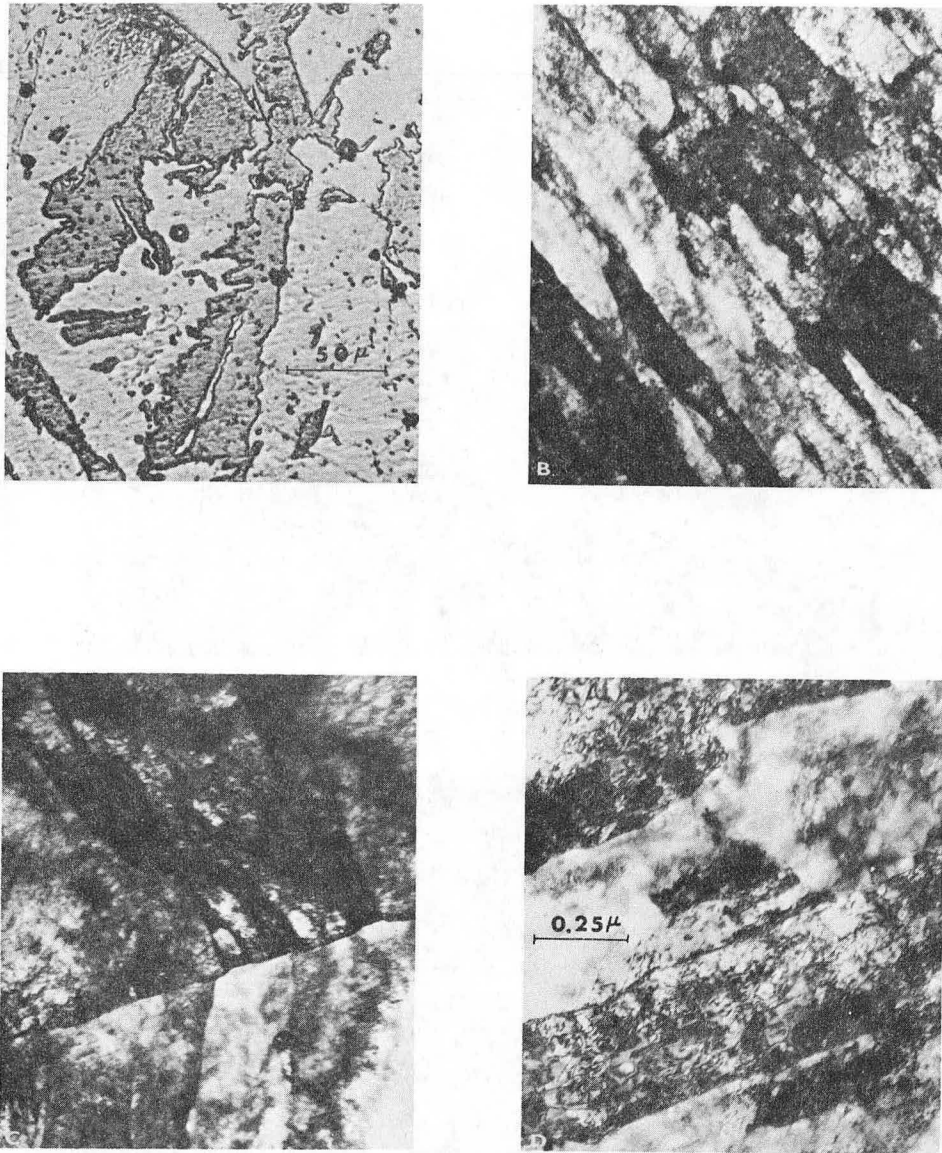
MUB-13761

Fig. 2 Hardness - aging time curves



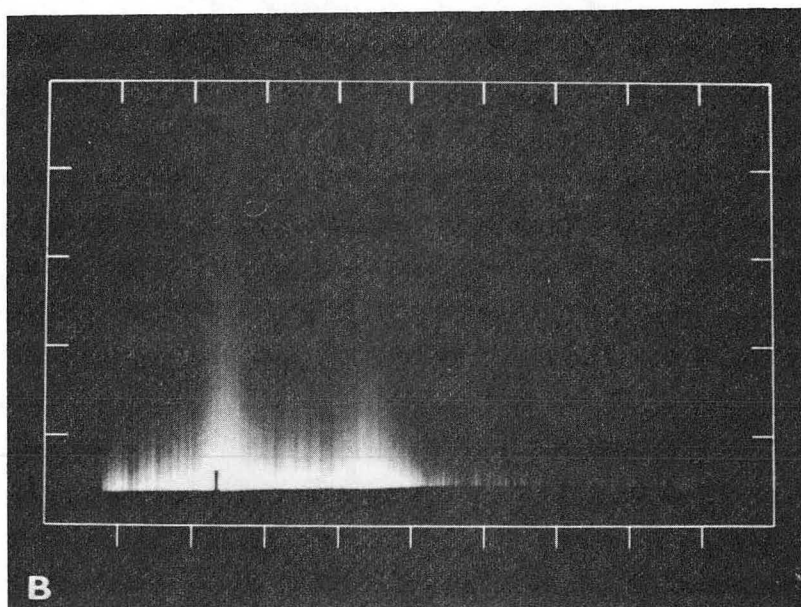
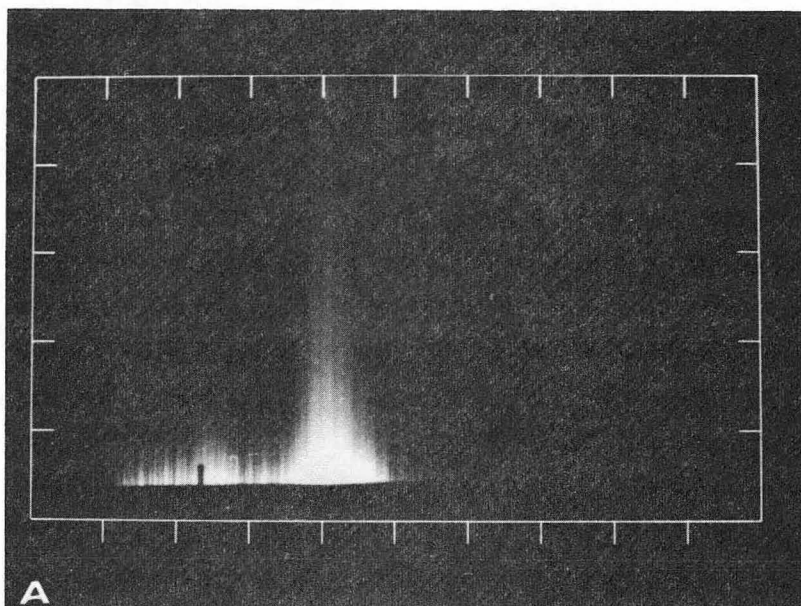
MUB-13760

Fig. 3 Stress-strain curves of the liquid nitrogen cooling state



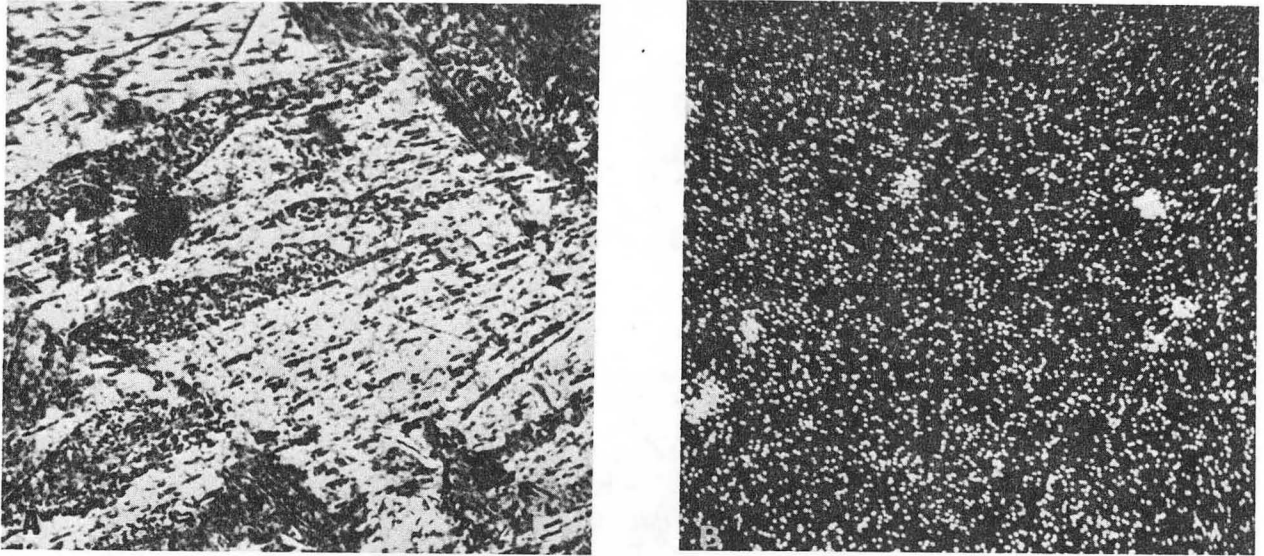
IM 2473

Fig. 4 As quenched states (2100°F annealing).
(A) Optical micrograph (water cooling), FeCl_3 etched
(B) Martensite platelets in L.N. cooling state, showing high dislocation density
(C) Nucleation of martensite on either side of grain boundary
(D) Substructural details of a martensite platelet



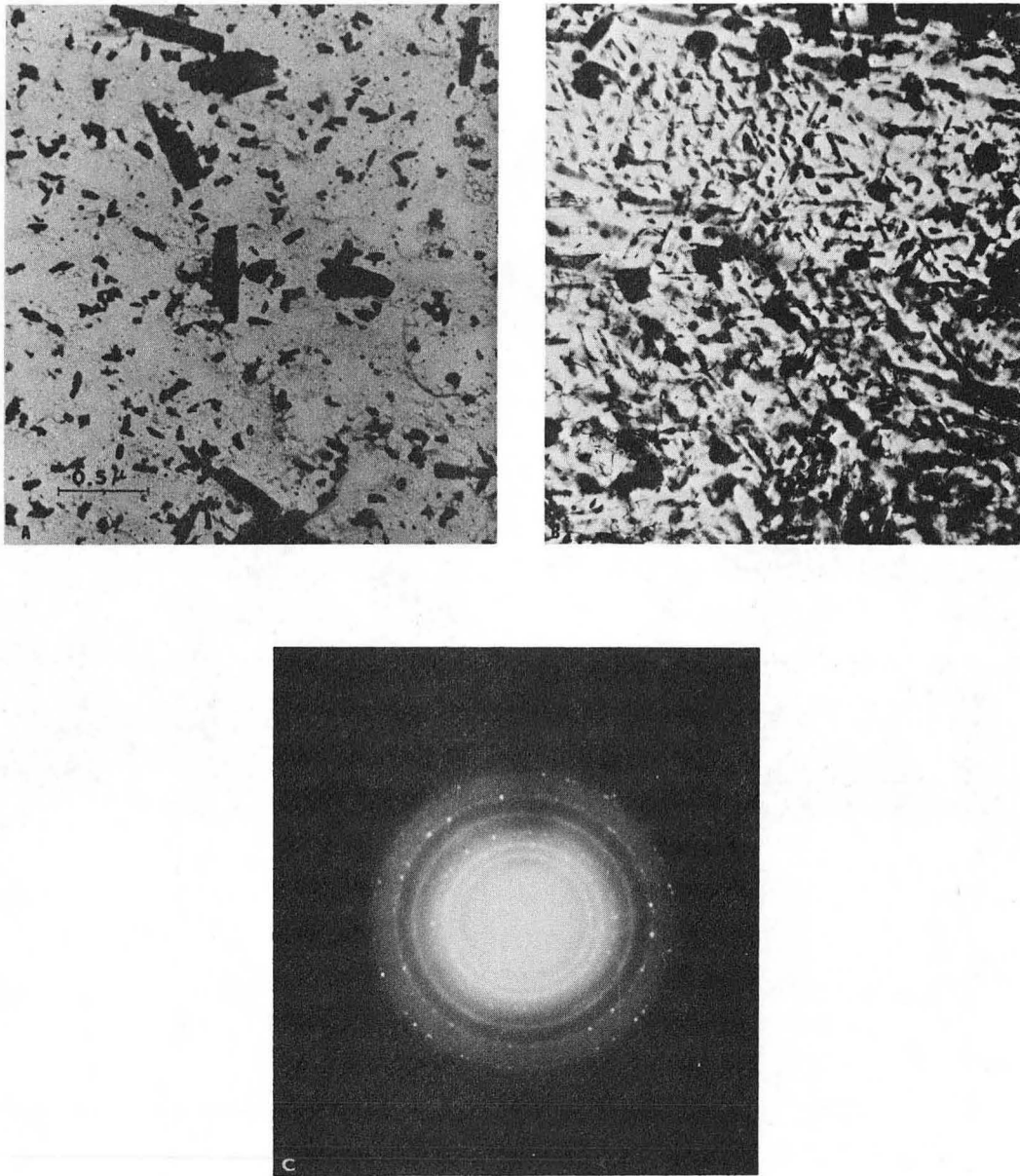
IM 2484

Fig. 5 X-ray microanalysis images showing that the precipitates are composed of Ni and Ti
(A) on Ni grid
(B) on Ti grid



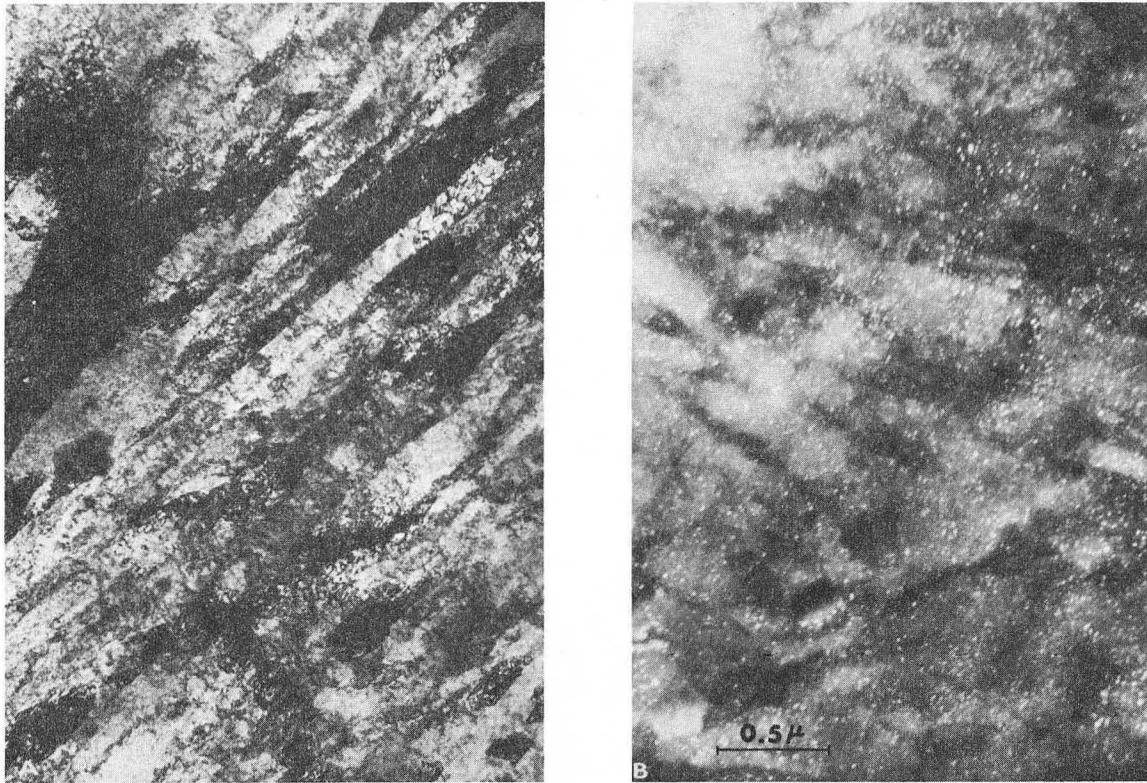
IM 2483

Fig. 6 X-ray image of the electron beam probe using TiK_{α}
(A) Optical photograph ($\times 550$)
(B) X-ray image of the area



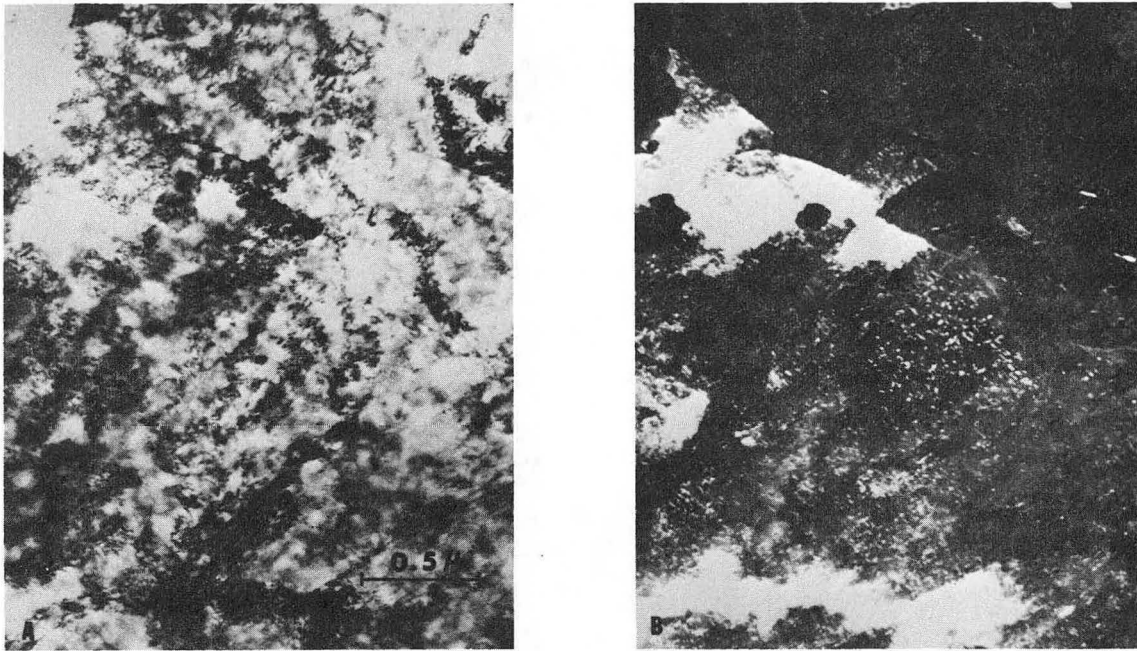
IM 2480

Fig. 7 (A) Carbon extraction replica
(B) Thin foil micrograph of an overaged specimen
(19.5 hrs aging)
(C) Selected area diffraction pattern from (A)



IM 2474

Fig. 8 2100°F/4 hrs L.N. quenched + 700°F/3 hrs aging
(A) Bright field
(B) Dark field, reveals the precipitates clearly



IM 2475

Fig. 9 2100°F/4 hrs + 700°F/12 hrs aging.
(A) Bright field
(B) Dark field showing growth of precipitates
and boundary precipitation

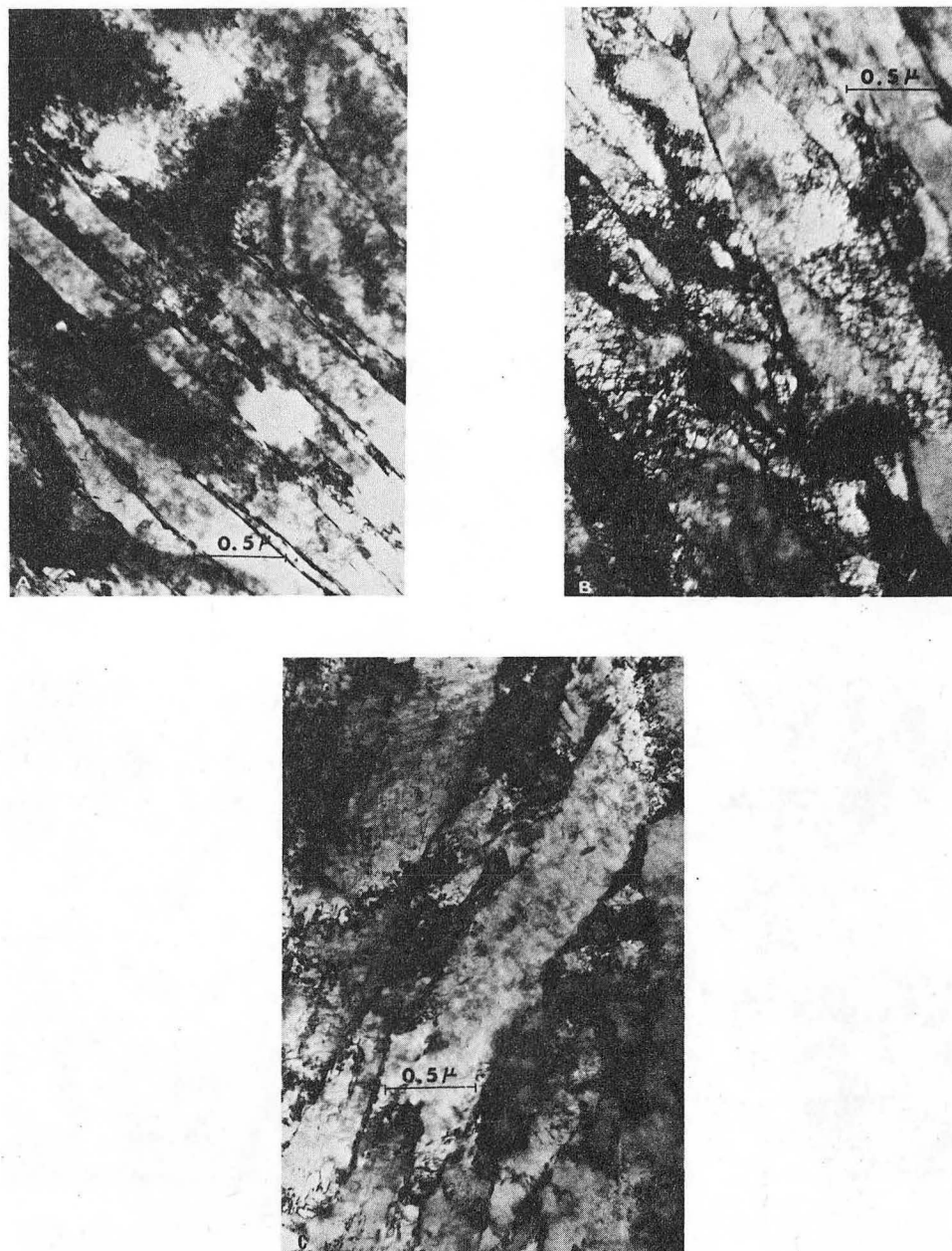
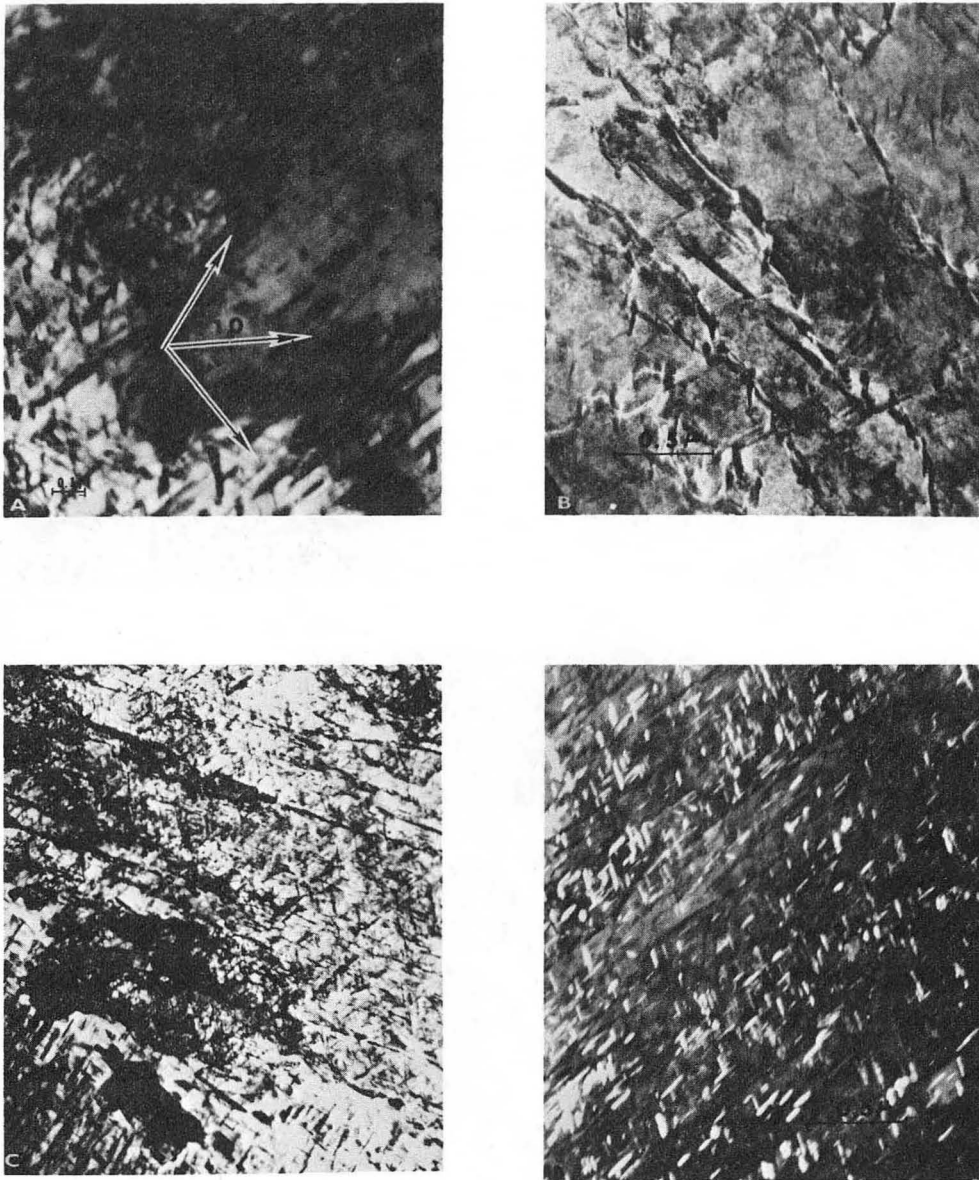
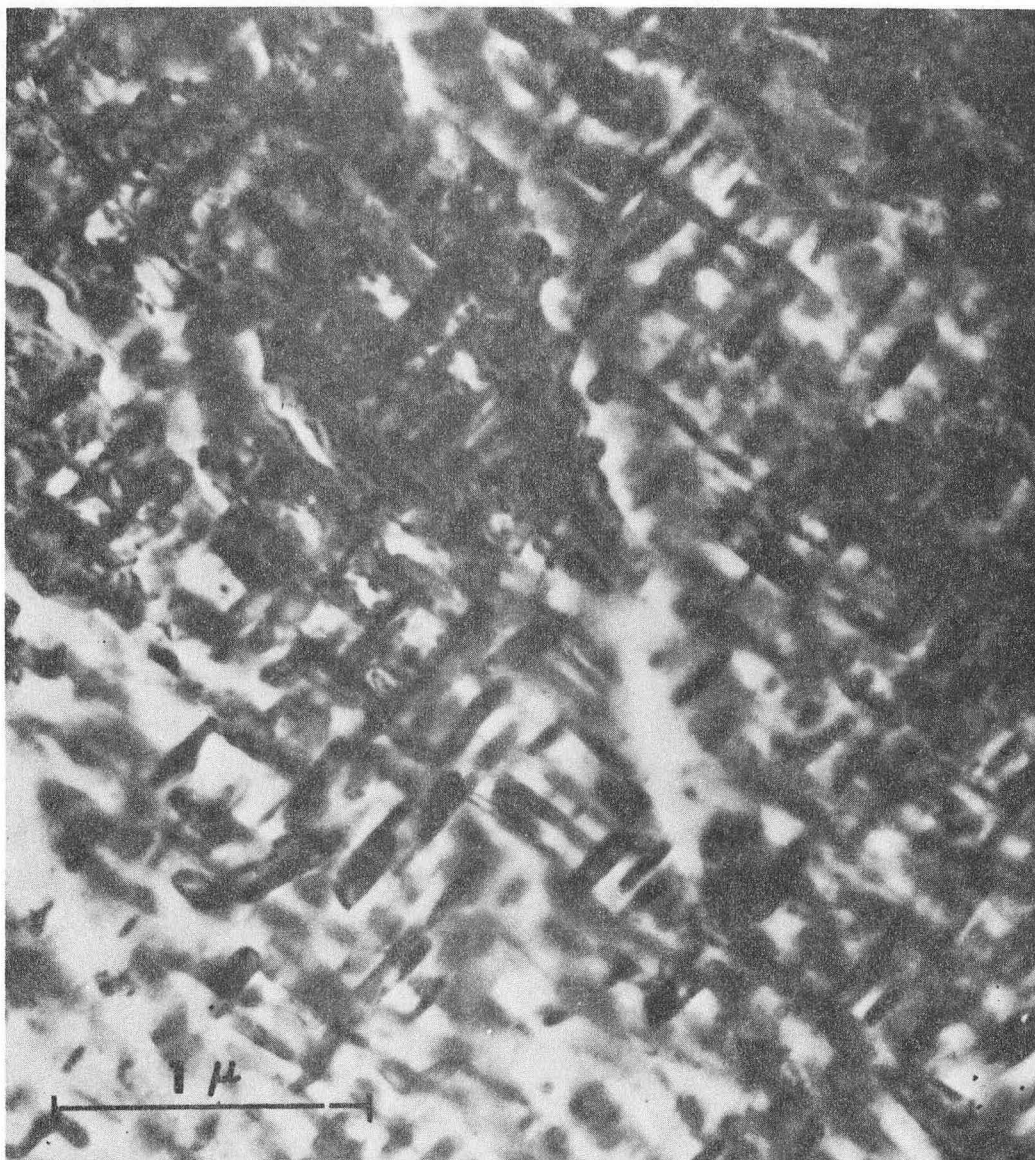


Fig.10 2100°F/4 hrs + 900°F/1 hr aging showing
boundary segregated precipitation
(A) L.N. cooled
(B) Furnace cooled
(C) Air cooled



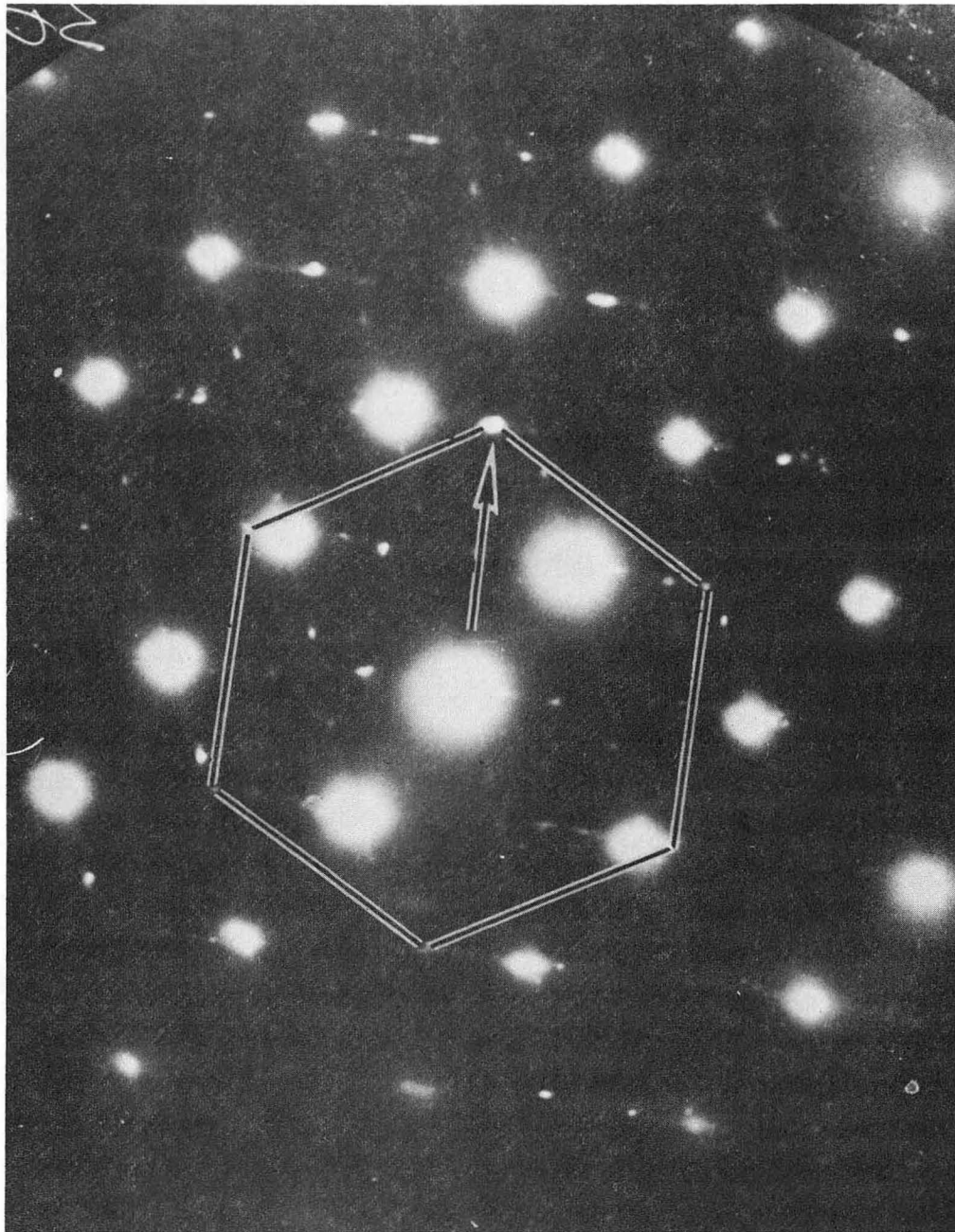
IM 2477

Fig. 11 2100°F/4 hrs + 900°F/3 hrs aging
(A) Morphology of precipitates
(B) Boundary precipitates
(C),(D) Bright and dark field micrographs



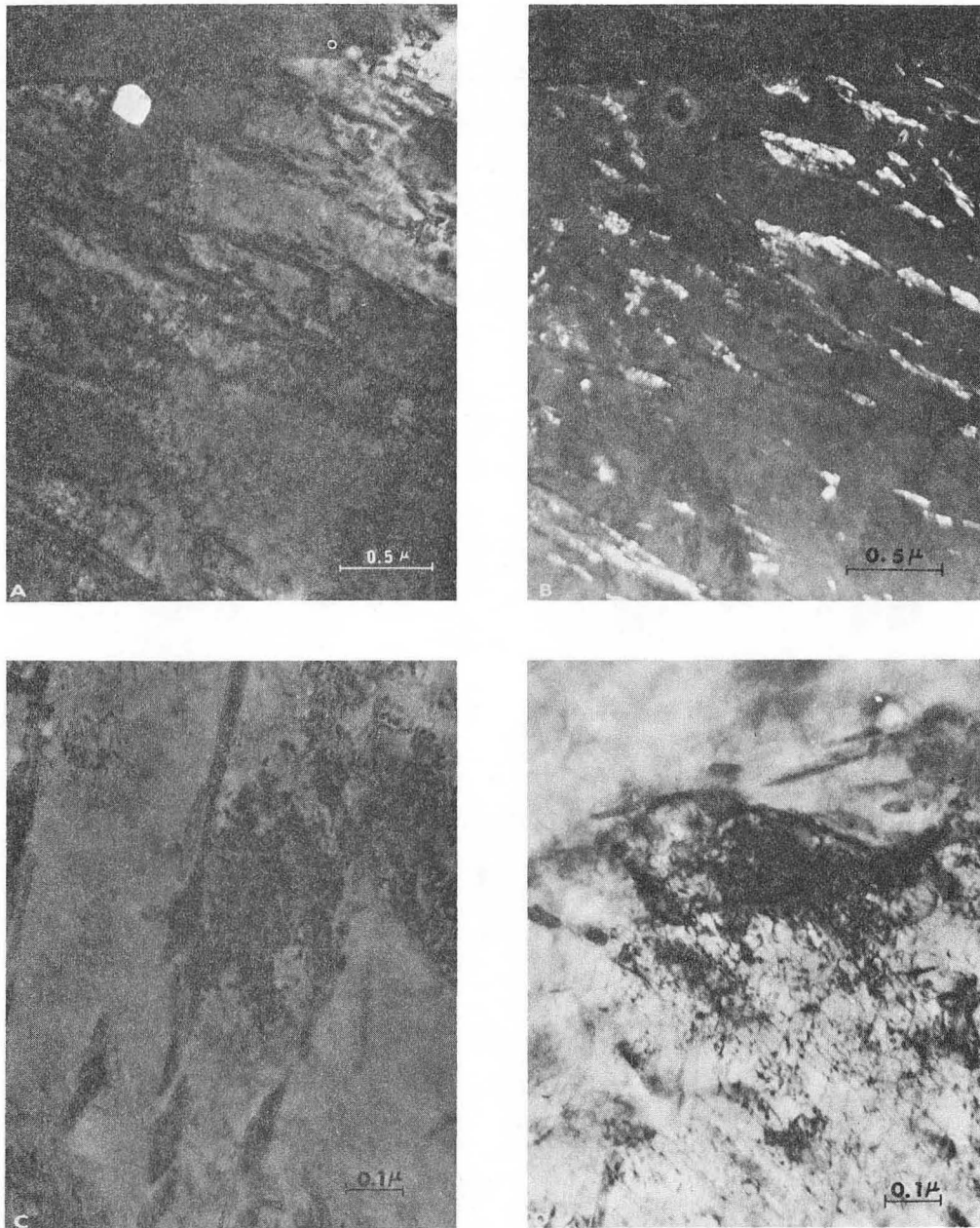
XBB 671-227

Fig. 12 2100°F/4 hrs + 900°F/12 hrs aging, showing growth of precipitates and formation of subgrains



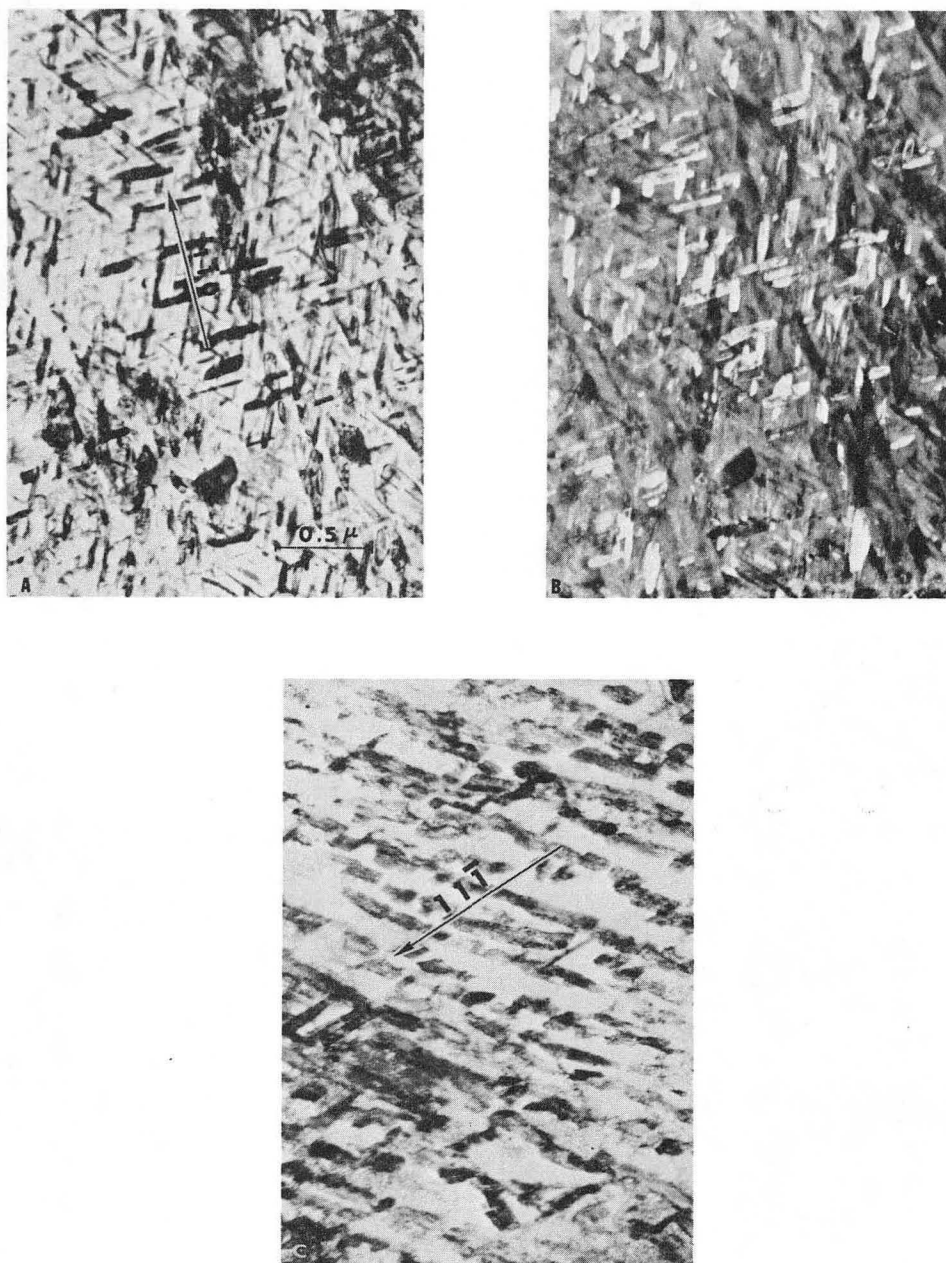
IM 2478

Fig. 13 Orientation relationships between precipitates and the matrix, shows $(001)_p // (110)_m$ $[200]_p // [\bar{1}\bar{1}]_m$



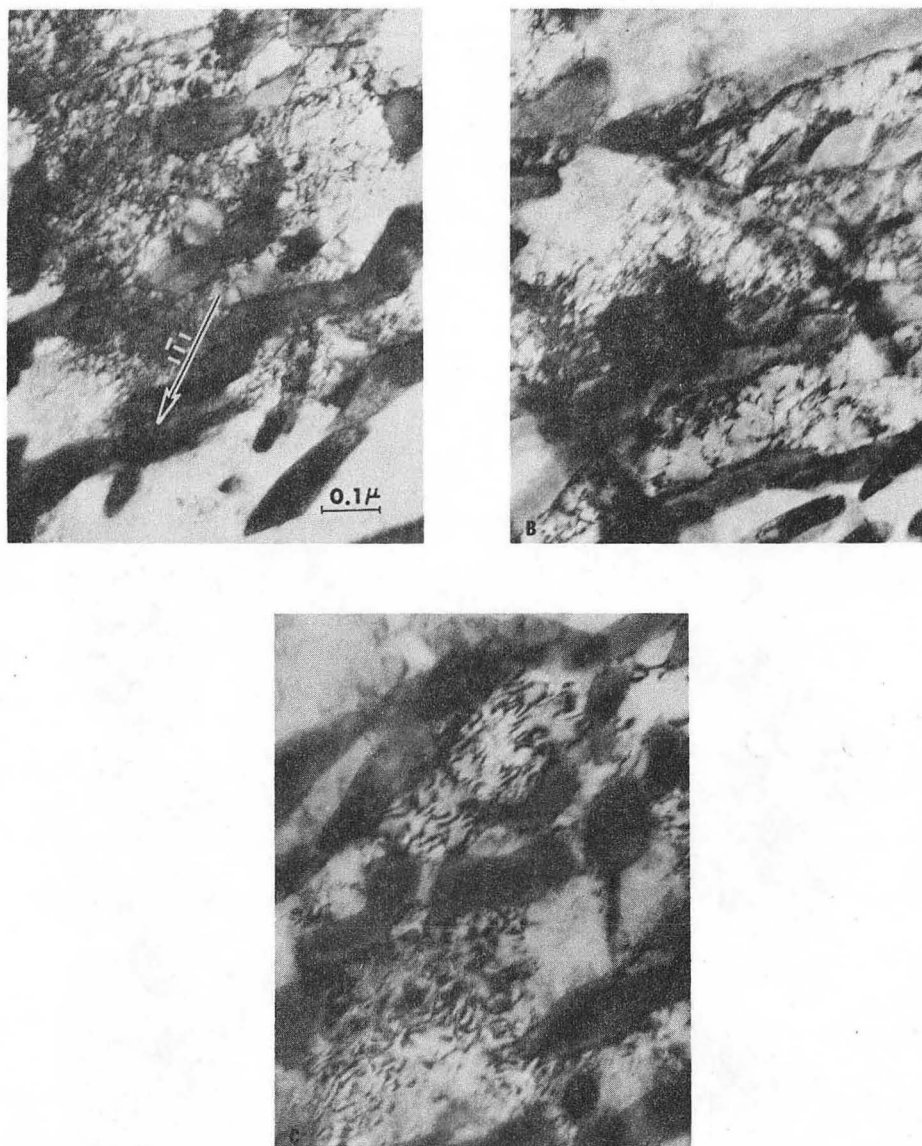
IM 2479

Fig. 14 Quenched + 900°F/1 hr aging, 30% deformed, showing (A), (B), (C) fragmentation of precipitates and (D) pile-up of dislocations against precipitates



IM 2481

Fig. 15 Quenched + 900°F/12 hrs aging, (A), (B) bright and dark field micrographs in the undeformed state, (c) after 30% deformation by rolling, showing shearing of boundary precipitates



IM 2482

Fig. 16 Quenched + 900°F/12 hrs aging, 30% deformed, showing bending and/or shearing of precipitates by dislocations



XBB 671-225

Fig. 17 2100°F/4 hrs + 700°F/1 hr aging. Some recovery of dislocations occurs.

This report was prepared as an account of Government sponsored work. Neither the United States, nor the Commission, nor any person acting on behalf of the Commission:

- A. Makes any warranty or representation, expressed or implied, with respect to the accuracy, completeness, or usefulness of the information contained in this report, or that the use of any information, apparatus, method, or process disclosed in this report may not infringe privately owned rights; or
- B. Assumes any liabilities with respect to the use of, or for damages resulting from the use of any information, apparatus, method, or process disclosed in this report.

As used in the above, "person acting on behalf of the Commission" includes any employee or contractor of the Commission, or employee of such contractor, to the extent that such employee or contractor of the Commission, or employee of such contractor prepares, disseminates, or provides access to, any information pursuant to his employment or contract with the Commission, or his employment with such contractor.

